



Eleventh U.S. National Conference on Earthquake Engineering
Integrating Science, Engineering & Policy
June 25-29, 2018
Los Angeles, California

EXPERIMENTAL INVESTIGATION ON ULTIMATE DRIFT CAPACITY OF RC BEAMS UNDER CYCLIC LOADING

S. Trivedi¹, N. Kurita², Y. Yoshida³, H. Shiohara⁴, and S. Tajiri⁵

ABSTRACT

In this report, the mechanism of strength loss at ultimate drift capacity in RC beams is investigated based on tests of twelve cantilevered RC beams with sufficient shear strength subject to multiple cycles of increasing lateral deflection. The specimens are one-third in scale and are designed with different values for the parameters including concrete compressive strength, longitudinal reinforcement content, shear-span ration, and spacing and yield strength of stirrups. An innovative method of instrumentation around the flexural hinge is presented which uses digital images of specimen surface, captured throughout the loading history. No significant improvement in drift capacity was observed by varying either of the stated parameter except stirrup spacing. Bulging of the concrete core with buckling-out longitudinal reinforcements was observed in most (but not all) cases. ASCE-41 recommendations for drift capacity of the tested specimens were found to result in largely conservative estimates and did not predict the influence of considered parameters correctly. Photogrammetric analysis also confirmed progressive bulging of the concrete core and build-up of large lateral expansion strains in the hinge region.

¹Ph.D. Candidate, Department of Architecture, University of Tokyo

²Graduate Student, Department of Architecture, University of Tokyo

³Undergraduate Student, Department of Architecture, University of Tokyo

⁴Professor, Department of Architecture, University of Tokyo

⁵Associate Professor, Department of Architecture, University of Tokyo

Trivedi S, Kurita N, Yoshida Y, Shiohara H, and Tajiri S. Tests on the drift capacity of RC beams under cyclic loading. *Proceedings of the 11th National Conference in Earthquake Engineering*, Earthquake Engineering Research Institute, Los Angeles, CA. 2018.



Eleventh U.S. National Conference on Earthquake Engineering
Integrating Science, Engineering & Policy
June 25-29, 2018
Los Angeles, California

Experimental investigation on ultimate drift capacity of RC beams under cyclic loading

S. Trivedi¹, N. Kurita², Y. Yoshida³, H. Shiohara⁴, and S. Tajiri⁵

ABSTRACT

In this report, the mechanism of strength loss at ultimate drift capacity in RC beams is investigated based on tests of twelve cantilevered RC beams with sufficient shear strength subject to multiple cycles of increasing lateral deflection. The specimens are one-third in scale and are designed with different values for the parameters including concrete compressive strength, longitudinal reinforcement content, shear-span ratio, and spacing and yield strength of stirrups. An innovative method of instrumentation around the flexural hinge is presented which uses digital images of specimen surface, captured throughout the loading history. No significant improvement in drift capacity was observed by varying either of the stated parameter except stirrup spacing. Bulging of the concrete core with buckling-out longitudinal reinforcements was observed in most (but not all) cases. ASCE-41 recommendations for drift capacity of the tested specimens were found to result in largely conservative estimates and did not predict the influence of considered parameters correctly. Photogrammetric analysis also confirmed progressive bulging of the concrete core and build-up of large lateral expansion strains in the hinge region.

Introduction

Earthquake resistant design philosophy in modern building codes is based on the idea of stable inelastic flexural response of ductile structural elements. Even in the appropriately designed and detailed structural elements, however, experimental evidence [1] indicates that application of successive loading cycles at ductile response leads to loss of resistance at a much lower drift level than that achieved with monotonic loading. Reliable and accurate assessment of this deformation capacity is crucial in effective realization of the performance based design philosophy.

Experimental investigations conducted in the past have commonly identified hoop spacing [2, 3] and applied loading history [4, 5] as parameters with the most significant influence on drift

¹Ph.D. Candidate, Department of Architecture, University of Tokyo

²Graduate Student, Department of Architecture, University of Tokyo

³Undergraduate Student, Department of Architecture, University of Tokyo

⁴Professor, Department of Architecture, University of Tokyo

⁵Associate Professor, Department of Architecture, University of Tokyo

Trivedi S, Kurita N, Yoshida Y, Shiohara H, and Tajiri S. Tests on the drift capacity of RC beams under cyclic loading. *Proceedings of the 11th National Conference in Earthquake Engineering*, Earthquake Engineering Research Institute, Los Angeles, CA. 2018.

capacity of RC beams. However, no clear understanding on the determining mechanism behind these observations has been established. Elwood and Moehle [6] and Pujol et al. [4] proposed empirical models to estimate drift capacity of columns based on the idea of degradation of shear carrying capacity of concrete with increasing flexural deformations. Another commonly considered mechanism is based on the idea of buckling of longitudinal reinforcement. Berry and Eberhard [7] established an empirical model to determine drift limit corresponding to the onset of bar buckling while Scribner [8] suggested design considerations to delay bar buckling associated loss of load resistance.

This report presents the findings from an experimental study of twelve RC beams conducted to understand the mechanism associated with loss of load resistance at ultimate drift capacity. In addition to conventional measurements, photogrammetry was used to record concrete surface deformations over a fine grid to ensure better understanding of concrete behavior than that possible with conventional contact based sensors.

Experiment Setup

Specimen design

A total of twelve beam specimens were designed considering a wide range of parameters expected to influence the ultimate drift capacity. All specimens were sized with a 180 mm × 240 mm section, representative of an approximately one-third scaled models of prototype beams in typical seismic resistant structures. Detailed section of the control specimen SB-01 is illustrated in Figure 1. Equal longitudinal reinforcement in the form of 4-D16 bars were provided on both faces. Transverse reinforcement was provided in the form of single hoops of D4 bar with 135° hooks arranged at with a uniform spacing of 60 mm throughout the loading span. No additional cross-ties were designed.

Considered parameters included *a*) concrete compressive strength, *b*) longitudinal reinforcement ratio, *c*) transverse reinforcement ratio, *d*) transverse reinforcement yield strength, and *e*) shear-span ratio. Specimens were designed by varying one or more of the parameters in SB-01 design. Only one variation in value was considered for each of the stated parameters as indicated in Table 1. The parameter variation adopted in respective specimen design is illustrated in the specimen matrix of Figure 2. For specimens in the SB-03 column group, higher longitudinal reinforcement ratio was achieved by providing additional 2-D16 bars in a second layer of reinforcement as expressed in Figure 1. For specimens designed with transverse reinforcement ratio as a parameter, larger reinforcement content was achieved by reducing the spacing of hoops to 30 mm. Finally, for the specimens designed with shear-span ratio as parameter, larger ratio was achieved by increasing the loading span to 1000 mm. Specifications of the used materials can be referenced in Table 1.

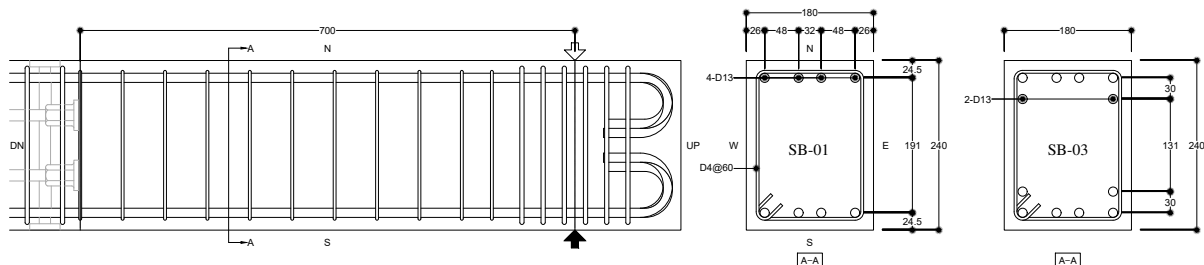
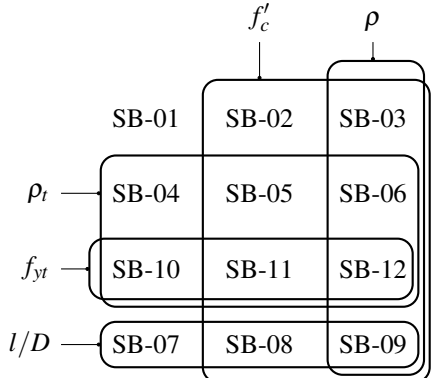


Figure 1: Specimen details (all dimensions are in mm)



f'_c : Concrete compressive strength
 ρ : Longitudinal reinforcement ratio
 ρ_t : Transverse reinforcement ratio
 f_{yt} : Transverse reinforcement yield strength
 l/D : Shear-span ratio

Figure 2: Parameter distribution

Parameter	SB-01	Variation
f'_c (MPa)	30*	60*
ρ (%)	1.29	1.94
ρ_t (%)	0.26	0.52
f_{yt} (MPa)	352†	869†
l/D	2.91	4.16
Longitudinal reinforcement:	SD345 (JIS G3112) ($f_y = 366 \text{ MPa}^\dagger$)	
Transverse reinforcement:	SD295 (JIS G3112) S45C (JIS G4051)	
* Target compressive strength of the casting batch		
† Average of tensile strength test of 5 bars		

Table 1: Specimen specifications

Loading setup

Specimens were subjected to alternate positive and negative loadings cycles to simulate an earthquake response. Loading was carried out using a system of pantograph frame and prestressing steel rods as indicated in Figure 3. Beam specimen was oriented in vertical position and the short stub portion was clamped using prestressing steel rods to stiff reaction stubs. Another set of prestressing steel rods were attached to the specimen tip and pantograph legs. A loading jack was used to apply horizontal force at the top of the pantograph. Thus, cantilever response was simulated between the tip of the specimen and the clamped portion. Deformation-controlled loading was applied with increasingly large target drifts, 3 loading cycles applied at each target drift.

Instrumentation

Load cells were attached to the end of each prestressing steel rods for load measurement. The total applied load at the beam tip can be simply given as the difference of steel rod forces in opposite directions as indicated in Figure 3. All specimen deformations were measured in reference to the specimen stub portion. Stiff reference frames were therefore attached to the specimen stub close to the critical section as shown in Figure 4. Total drift ratio (Δ) at the tip can be deduced using laser displacement sensor measurements (δ_1 and δ_2) as:

$$\Delta(\%) = \frac{\delta_1 + \delta_2}{2} \times \frac{100}{l} \quad (1)$$

Rotation at the hinge region (θ_{hinge}) and axial strain (ϵ_{axial}) can also be calculated using laser displacement sensor measurements (δ_3 and δ_4) as:

$$\theta_{hinge}(\text{rad}) = \tan^{-1} \left(\frac{\delta_3 - \delta_4}{d_2} \right) \quad (2)$$

$$\epsilon_{axial}(\%) = \frac{\delta_3 + \delta_4}{2} \times \frac{100}{d_3} \quad (3)$$

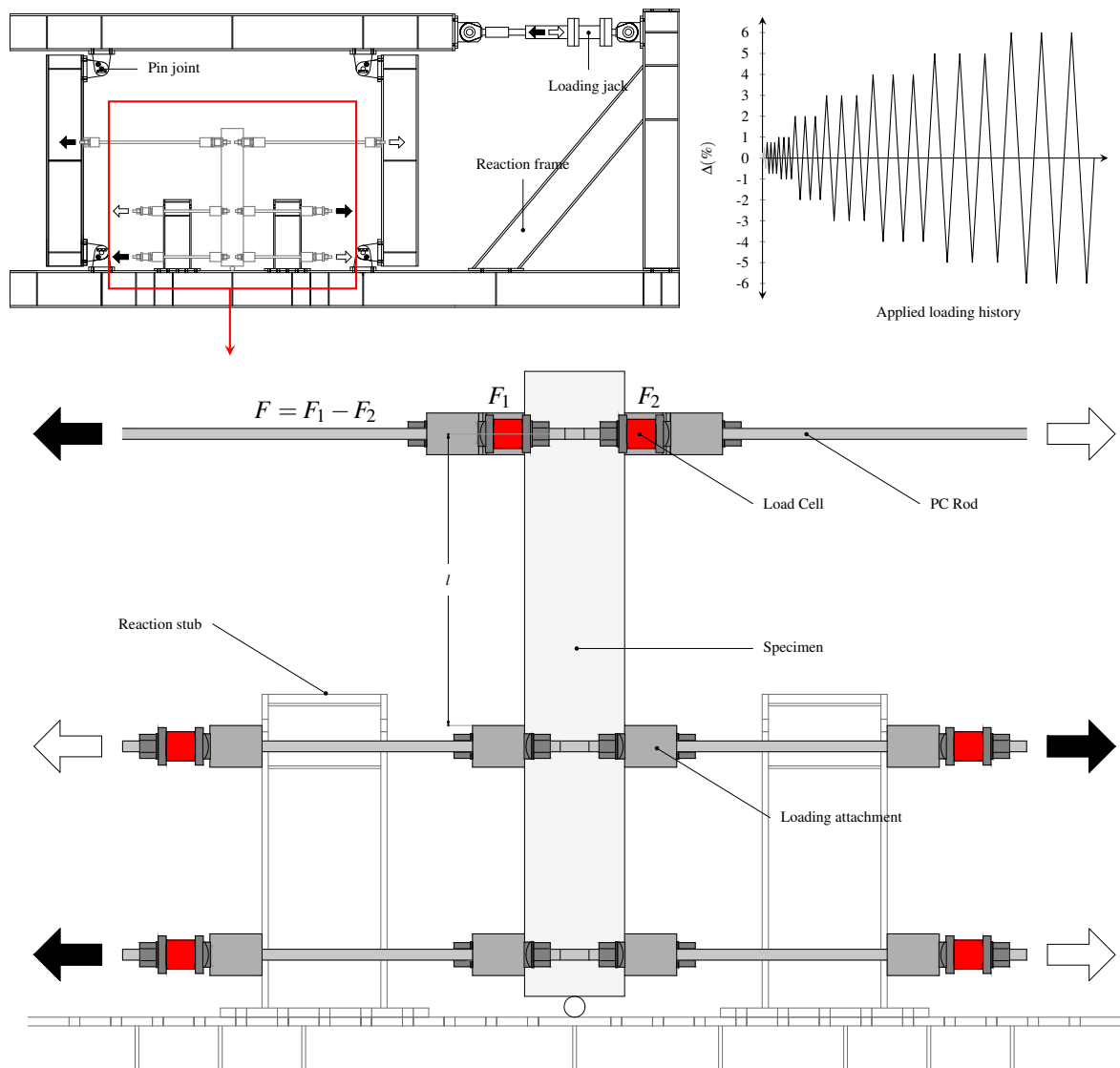


Figure 3: Loading setup

Photogrammetric measurements were calculated by post-processing the stream of digital images captured throughout the experiment using the setup shown in Figure 4. Photographed surface was installed with a fixed print-pattern on a $50\text{ mm} \times 50\text{ mm}$ grid as expressed in Figure 5. A pattern-matching technique [9] was used to digitally identify the marked locations and measure corresponding deformations.

Experiment Results

General behavior

All specimens developed stable flexural response after yielding in both directions and continued to resist the applied load for multiple loading cycles at large target drift as the longitudinal reinforcements strain-hardened. Variable response was however observed as the specimens started to exhibit strength deterioration. Some common observations are illustrated in Figure 6. Specimen SB-01 exhibited well distributed flexural cracks in the hinge zone as well as large

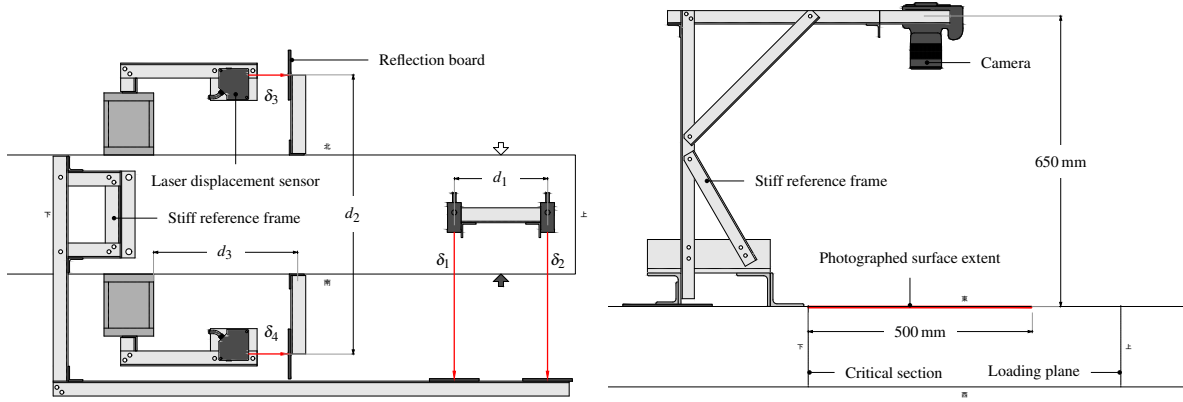


Figure 4: Measuring scheme (*left*: Displacement measurements; *right*: Photogrammetric measurements)

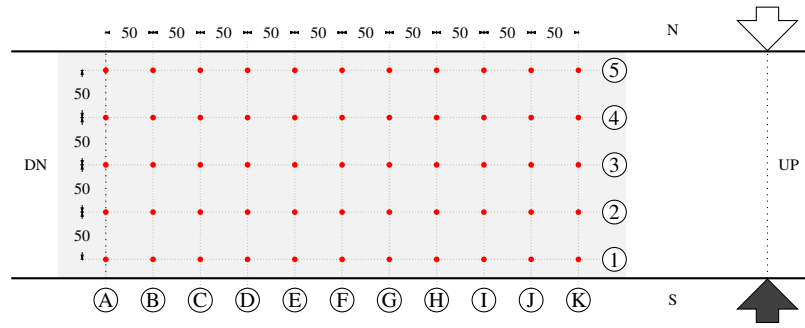


Figure 5: Photogrammetric measurement grid

inclined shear cracks before ultimately loosing resistance accompanied by widening of the inclined cracks. Specimen SB-04, designed with twice as much stirrups, exhibited closely spaced flexural cracks in the hinge zone but the inclined cracks developed at a shallower angle and spread to a smaller length as compared to SB-01. Specimen SB-07, with a larger shear-span ratio, developed fewer flexural cracks that were near vertical and a prominent diagonal crack that widened significantly with increasing loading cycles and led to loss of resistance. Another common feature observed at the end of loading in quite a few specimens was the bulging of longitudinal bars often accompanied with opening of stirrups as clearly seen in the case of SB-05. Specimens with an additional layer of reinforcement also exhibited similar bulging in an especially pronounced manner for the inner layer of reinforcement which was not bound with stirrups. However, bulging phenomenon was not universally observed as illustrated in the case of SB-12 which exhibited near horizontal shape of longitudinal bars at the end of loading.

Moment-drift response

Moment-drift response obtained for each specimen is expressed in Figure 7. All specimens exhibited some degree of strength gain after yielding due to strain hardening in the longitudinal reinforcements before resulting in loss of resistance, typically at some point after loading cycles at 3 % target drift. Specimen group (SB-04 to SB-06 and SB-10 to SB-12) with closely spaced transverse reinforcement resulted in superior drift capacities, sustaining resistance for loading cycles at 5 % target drift. Specimens with high-strength concrete did not show any significant improvement in the drift level sustained before loss of resistance but did result in a more gradual deterioration in strength upon further loading. Specimen group (SB-03, SB-06, SB-09 and SB-12) with longitudinal reinforcement in a second layer resulted inferior drift capacities. As

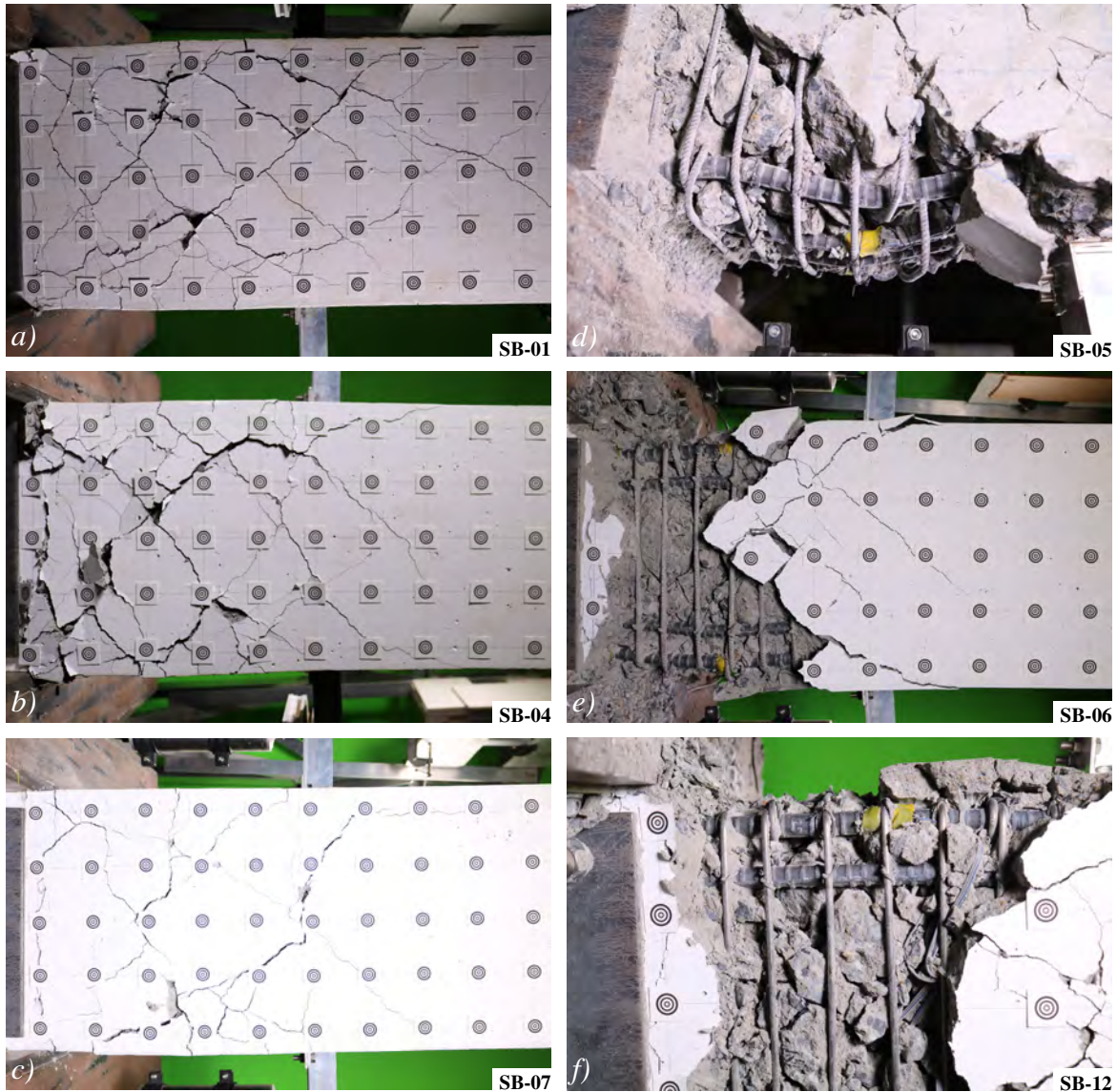


Figure 6: General behavior: *a)* SB-01 at the end of 3 cycles of loading at 3 % target drift; *b)* SB-04 at the end of 3 cycles of loading at 4 % target drift; *c)* SB-07 at the end of 2 cycles of loading at 3 % target drift; *d)* SB-06 at the end of 3 cycles of loading at 5 % target drift; *e)* SB-05 at the end of 3 cycles of loading at 6 % target drift; *f)* SB-12 at the end of 3 cycles of loading at 5 % target drift;

discussed previously, this may be attributed to insufficient lateral restraint provided to the bars in second layer. Specimens (SB-07 to SB-09) with a larger span to depth ratio resulted in almost similar drift capacities. Specimen group (SB-10 to SB-12) with closely spaced stirrups of high strength steel did not result any improvement over the drift capacities observed in the ordinary strength stirrup specimen group (SB-04 to SB-06).

Moment-rotation response

Local rotation measured at the hinge is expressed against the applied moment in Figure 8 for all the specimens except SB-01 for which data could not be recorded due to sensor failure. All specimens exhibited a skewed response in positive and negative loading directions, especially for large target drift cycles, often accompanied with deterioration in strength.

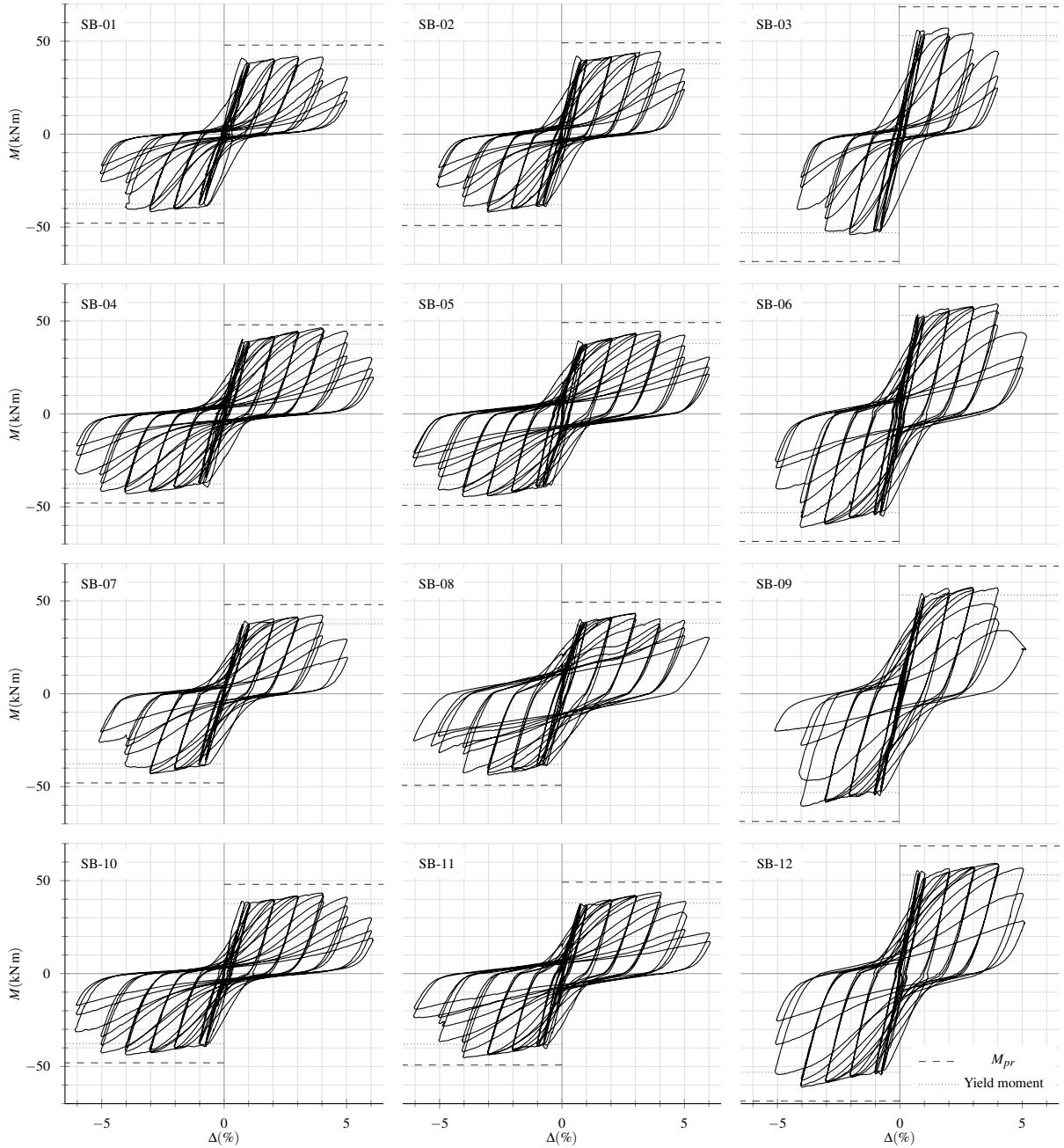


Figure 7: Moment-drift response (M_{pr} calculated as per ACI 318 [10] and moment at yield calculated using equivalent stress block approach with actual material strength values)

Generalized force-deformation relation for concrete elements as defined by Clause 10.3.1.2.2 and Table 10-7 of ASCE 41 [11] is also expressed in the same figure for comparison. All specimens were assumed to be controlled by flexure and for symmetrically reinforced sections $(\rho - \rho')/\rho_{bal}$ was taken as 0. Conformity or non-conformity of the transverse reinforcement, value of the parameter $V/b_w d \sqrt{f'_c}$ (denoted by v_x) and the resulting value of modeling parameters a and b (in rad) are indicated in the figure for each specimen. Residual strength ratio parameter c takes the value of 0.2 for all the specimens. Ultimate drift capacity before loss of resistance calculated according to ASCE 41 results in conservative estimates for almost all the specimens. These estimates appear especially conservative for specimens with high-strength concrete and high-strength transverse reinforcement.

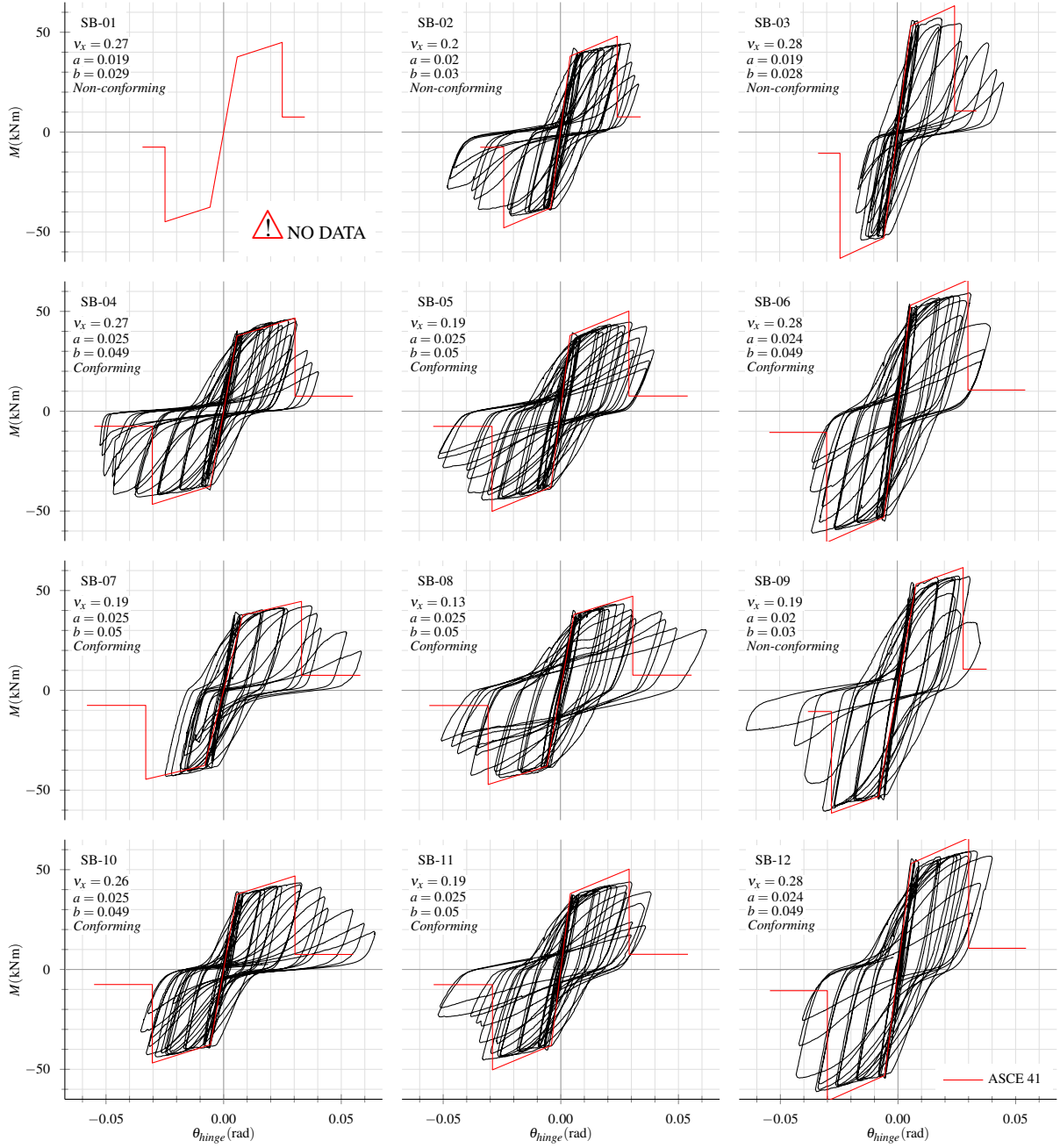


Figure 8: Moment-rotation response

Photogrammetric measurements

Photogrammetric analysis was used to record the displacement trace of targets at typical grid locations shown in Figure 5. Lateral strains at each vertical grid (A-to-K) were calculated using the relative deformation between the extreme points (e.g. A1 and A5 for grid A) on each grid as expressed in Figure 9. Strains at large target drift cycles could not be calculated due to loss of photogrammetric targets with progressive concrete surface cracking. Barreling of concrete core with increasingly large target drift cycles is clearly evident in all specimens. The extent over which barreling was observed was largest in SB-01 while more concentrated lateral expansion was observed in SB-04 and SB-10. Specimen SB-07 exhibited least barreling expansion in the hinge region.

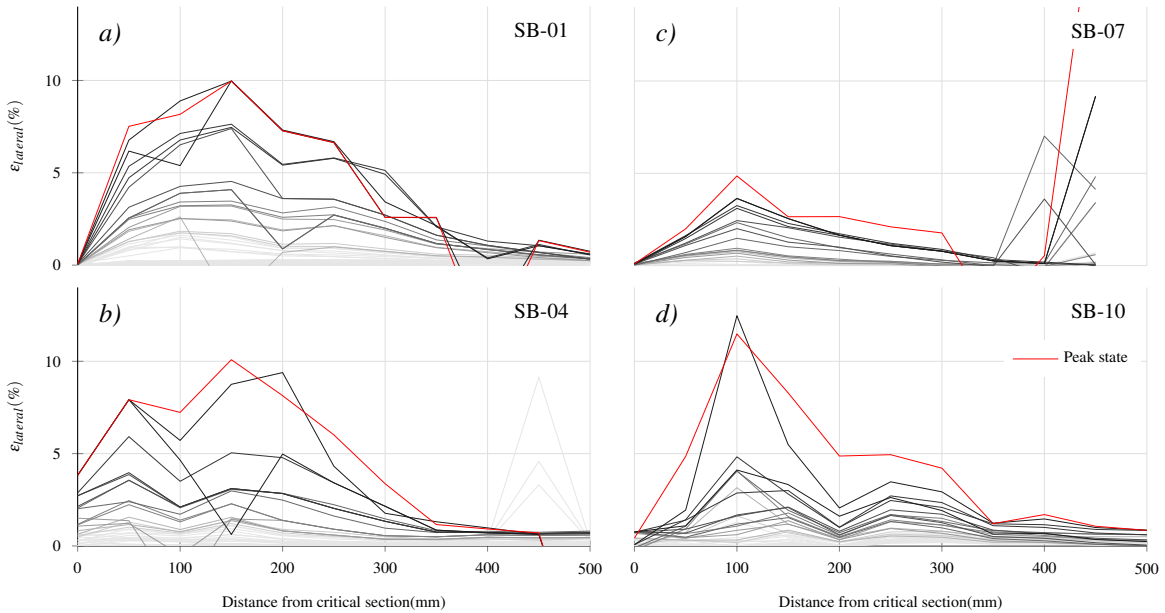


Figure 9: Lateral strain recorded at the photogrammetric grids: *a)* Specimen SB01 until 2 cycles 4 % target drift; *b)* Specimen SB04 until 2 cycles 5 % target drift; *c)* Specimen SB07 until 3 cycles 3 % target drift; *d)* Specimen SB10 until 3 cycles 4 % target drift

Summary and Conclusions

Twelve RC beams designed with different concrete strengths, longitudinal reinforcement ratio, transverse reinforcement ratio, shear-span ratio and transverse reinforcement strength were tested to investigate ultimate drift capacity under cyclic loading. Major findings can be summarized as follows:

1. Enhancement of transverse reinforcement ratio was found to be the most influential parameter affecting ultimate drift capacity.
2. High-strength concrete and high strength transverse reinforcement did not result in any significant ultimate drift capacity improvement.
3. ASCE 41 estimates of ultimate drift capacities were found to be largely conservative.
4. Photogrammetry could be successfully implemented to record concrete surface deformations, albeit data recordings were limited by excessive cracking at large deformations.

Acknowledgements

The authors wish to express their gratitude to the Grants-in-Aid for Scientific Research (JSPS KAKENHI) under Grant No. JP16H04446 for the financial support of the research. The first author gratefully acknowledges the Japanese Government MEXT scholarship program.

References

1. J. M. Ingham, D. Liddell, and B. J. Davidson. Influence of Loading History on the Response of a Reinforced Concrete Beam. *Bulletin of the New Zealand Society for Earthquake Engineering*, 34(2):107–124, 2001.

2. Tea Visnjic, Grigoris Antonellis, Marios Panagiotou, and Jack P. Moehle. Large Reinforced Concrete Special Moment Frame Beams under Simulated Seismic Loading. *ACI Structural Journal*, 113(03):469–480, 2016. doi: 10.14359/51688193.
3. Yan Xiao and Rui Ma. Seismic behavior of high strength concrete beams. *The Structural Design of Tall Buildings*, 7(1):73–90, 1998.
4. Santiago Pujol, Mete A. Sozen, and Julio A. Ramirez. Displacement History Effects on Drift Capacity of Reinforced Concrete Columns. *ACI Structural Journal*, 103(2):253–262, 2006. doi: 10.14359/15183.
5. I-Kuang Fang, Chuen-Shyuan Wang, and Keh-Luen Hong. Cyclic behavior of high-strength concrete short beams with lower amount of flexural reinforcement. *ACI Structural Journal*, 91(1):10–18, 1994. doi: 10.14359/4477.
6. Kenneth J. Elwood and Jack P. Moehle. Drift capacity of reinforced concrete columns with light transverse reinforcement. *Earthquake Spectra*, 21(1):71–89, 2005. doi: 10.1193/1.1849774.
7. Michael P. Berry and Marc O. Eberhard. Practical performance model for bar buckling. *Journal of Structural Engineering*, 131(7):1060–1070, 2005. doi: 10.1061/(asce)0733-9445(2005)131:7(1060).
8. Charles F. Scribner. Reinforcement Buckling in Reinforced Concrete Flexural Members. *ACI Structural Journal*, 83(6):966–973, 1986. doi: 10.14359/2648.
9. Sei Nagashima, Takafumi Aoki, Tatsuo Higuchi, and Koji Kobayashi. A subpixel image matching technique using phase-only correlation. In *Proceedings of the 2006 International Symposium on Intelligent Signal Processing and Communications*, pages 701–704, Tottori, Japan, 2006. IEEE. doi: 10.1109/ISPACS.2006.364751.
10. ACI 318. *Building Code Requirements for Structural Concrete*. American Concrete Institute, Farmington Hills, MI, 2014. ISBN 978-1-942727-11-8.
11. ASCE 41. *Seismic Evaluation and Retrofit of Existing Buildings*. American Society of Civil Engineers, Reston, VA, 2013. ISBN 978-0-7844-7791-5.